Control of pentacene thin film growth by supersonic molecular beam deposition

Wu, Yu

Chapter 3

Initial growth of pentacene controlled by the kinetic energy of the incident molecules *

This chapter presents a systematic investigation of the correlation between kinetic energy of the incident molecules (E_k = thermal energy, 3.3, 5.0, 6.4 and 6.7 eV) and initial growth mode of the pentacene submonolayer on the silicon oxide surface by using the supersonic molecular beam deposition (SuMBD). We found that the molecular kinetic energy plays a very important role in determining the critical nucleus size, the formation of the molecular island, the crystalline quality of first completed monolayer and even the growth mode of the subsequent layers. With increasing $E_k \geq 5.0$ eV, the morphology in the submonolayer regime evolves towards the higher island density with smaller island size. SuMBD grown molecular islands present a less fractal structure and smoother island edges than those resulting from organic molecular beam deposition (OMBD). The critical nucleus size was determined in the low coverage regime by using the general scaling function and showed a transition from 3 to 2 pentacene molecules when the kinetic energy of the incident molecules exceeded 5-6 eV. With respect to pentacene islands grown by OMBD, those resulting from SuMBD are more anisotropic in shape, and more uniform in size, pointing to correlated island growth. Moreover, for OMBD 3D island growth is observed while SuMBD gives rise to the Stransky- Krastanov growth in the pentacene initial growth. By comparing atomic force micrographs of the height and of the net transverse shear force, we established that when $E_k \geq 5.0$ eV, the first monolayer is composed of large single crystalline domains which extend over up to 10 micron. In these growth conditions not only the surface diffusivity is high, but energy dissipation occurring when the molecules hit the surface seems to lead to the reorientation of whole islands during island coalescence, resulting in the elimination of grain boundaries. The pentacene initial growth by SuMBD was interpreted by the diffusion mediated growth model and the conditions for pentacene initial growth were optimized.

* This chapter is based on Yu Wu, Tullio Toccoli, Norbert Koch, Erica Iacob, Alessia Pallaoro, Petra Rudolf and Salvatore Iannotta, "Controlling the early stages of pentacene growth by supersonic molecular beam deposition" published on Physics Review Letter 98, 076601 (2007) and based on Yu Wu, Tullio Toccoli, Jian Zhang, Norbert Koch, Erica Iacob, Alessia Pallaoro, Salvatore Iannotta and Petra Rudolf, "Key role of molecular kinetic energy in early stages of pentacene island growth" submitted to Applied Physics A.

3.1 Introduction

Pentacene is one of the most promising candidates for organic electronics applications [1] and recently very high hole mobilities (up to 5.5 cm^2/Vs) [2] have been achieved in pentacene thin film based field effect transistors. Nonetheless, the difficulty in determining and controlling key properties such as structure, morphology and interfaces of the organic layer is still a major factor limiting the electronic properties. The charge mobility is a crucial parameter for device performance and previous studies have demonstrated that it is highly sensitive to the crystallinity of the deposited pentacene thin film, *i.e.* to the grain size [3, 4], defect density [5, 6] and crystal polymorph [7 , 8]. In particular, further progress in device development requires the production of highly ordered large size pentacene crystals [9], possibly eliminating grain boundaries [1,]. In the past few years, several studies based on the OMBD grown pentacene layers have demonstrated that the pentacene grain size can be modulated via changing the deposition rate, the substrate temperature or modifying the substrate surface with organic self assembled layers [10, 11, 12, 13, 14]. Recent reports illustrated that supersonic molecular beam methods [15, 16, 17] represent a viable and promising approach to improve the pentacene crystallinity based on the idea of tuning and controlling the energy of the incident molecules. Since the film quality is determined by the early stages of growth and since the first few molecular layers are crucial for charge transport in organic thin film transistors (OTFTs) [18, 19], we focused our studies on the submonolayer regime on a chemically inert, flat SiO_x/Si surface. Recently, Killampalli *et al.* [20] studied the deposition of pentacene monolayers on SiO_x/Si by supersonic molecular beams at various kinetic energies (1.5-6.7 eV). They reported an adsorption probability that decreases for increasing incident kinetic energy, an island density that did not change appreciably during island growth, and the critical nucleus size requires four molecules. On the other hand, studies of thermally sublimated pentacene grown on SiO_x find a critical nucleus size of three [21, 22].

In this work, we show that, by carefully tuning flux and energy of the incident molecules, one can establish the correlation between kinetic energy of incident pentacene and morphology of the deposited pentacene submonolayers at different growth stages. In particular, we demonstrate that at moderate fluxes: a) the island density depends markedly on the kinetic energy; b) the critical nucleus size determined by applying the

general scaling function [23], has a transition from 3 to 2 when the E_k > 5-6 eV; c) with increasing E_k correlated island growth becomes more pronounced and the island structure changes from fractal to less fractal and becomes anisotropic; d) Stransky- Krastanov growth mode is observed in the pentacene initial growth. With the help of transverse shear microscopy (TSM) we could establish the conditions for producing highly ordered pentacene layers containing large single crystal grains and a minimum density of grain boundaries. Although a polycrystalline structure is found for all pentacene monolayers, the single crystal grain size strongly depends on the kinetic energy of the impinging molecules and reaches up to ~10 μm for the sample grown at E_k = 6.4 eV.

3.2 Pentacene submonolayer growth on SiO_x by supersonic molecular beam deposition

3.2.1 SiO_x substrate preparation

To obtain a clean silicon oxide surfaces with few impurities and defects, SiO_x layers were prepared by wet chemical oxidation of silicon wafers (Si(100), p-type with boron dopant, resistivity 1 to 10 Ω cm^{-1}, purchased from Silicon Quest International, USA). Before subjecting them to chemical oxidation, the silicon wafers were cleaved into 15 mm × 13 mm pieces and initially cleaned by sonication in de-ionized water (Milli-Q, 18.0 MΩ) and in acetone (analytical reagent A.R., Labscan Ltd, Ireland) for 15 min. Then, they were transferred to a fresh acetone bath and heated to the boiling point for 15 min in order to remove the impurities from the surface. The chemical oxidation process comprised the following steps: 1) after the general cleaning, the samples were transferred to a H_2SO_4 (97%, pro analysi, Merck, Germany): H_2O_2 (30% Merck, Germany) = 1:3 solution and heated up to ~ 70° for 30 min. Samples were then cleaned by de-ionized water for several times and the surface became totally hydrophilic. 2) Samples were transferred into HCL (37%, pro analysi, Merck, Germany) + H_2O_2 (1:1) piranha solution and heated up to 30° for 15 min. This was a very strong chemical reaction producing a large amount of visible gas bubbles. Finally, samples were again repeatedly washed by de-ionized water to remove any solution traces. To avoid contamination through

prolonged exposure to the air, the substrates were stored in a small vacuum chamber before using them for pentacene submonolayer growth. This treatment resulted in very thin (~ 3 nm) SiO_x layers, as determined by ellipsometry measurements.

These SiO_x substrates showed a relatively low root mean square roughness of ~ 0.5-1 nm as measured by atomic force microscopy in tapping mode on the freshly prepared surface. However, a few bright spots (area density of ~ $2.5\times10^7/cm^2$) presumably due to contamination still showed up in AFM images. To check the hydrophilicity of the substrates, the contact angles were measured in air by using the sessile drop method [24] in a custom built microscope-goniometer system. A 1.25 μl drop of de-ionized water was deposited onto the freshly prepared SiO_x substrate surface using a Hamilton micro-syringe and the contact angle was measured after 60 s. For each surface, we collected data at four different places in order to check the uniformity of surface polarity and to calculate the average contact angle. All substrates showed contact angles of 35 ± 2° and are therefore hydrophilic.

3.2.2 Characterization of the supersonic molecular beam by time of flight mass spectroscopy

Time of flight mass (ToF) spectroscopy was employed to characterize the generated supersonic molecular beams, namely to ascertain that no chemical impurities or molecular clustering were present in the beam and to determine the average molecular velocity and hence the kinetic energy of the molecules in the beam. Figure 3-1 (a) shows the ToF spectra recorded for beams with three different kinetic energies. Based on the relation between the flight time and the charge/mass ratio of the photo-ionized molecules, pentacene is identified as the only chemical component in all beams. Pentacene molecular isotopes are recognized as small shoulders on the right of the main peaks. There is no any evidence of pentacene molecular clusters, which would be identifiable by a larger mass. The peaks corresponding to the three molecular beams are centered at 37.04 μs, 37.14 μs and 37.26 μs, from which mean kinetic energies of 6.4 eV, 5.0eV and 3.3 eV are deduced. The signal of the molecular beam with kinetic energy of 6.4 eV shows a full width at half maximum (FWHM) of 0.04 μs, indicative of a narrow molecular velocity distribution. On the

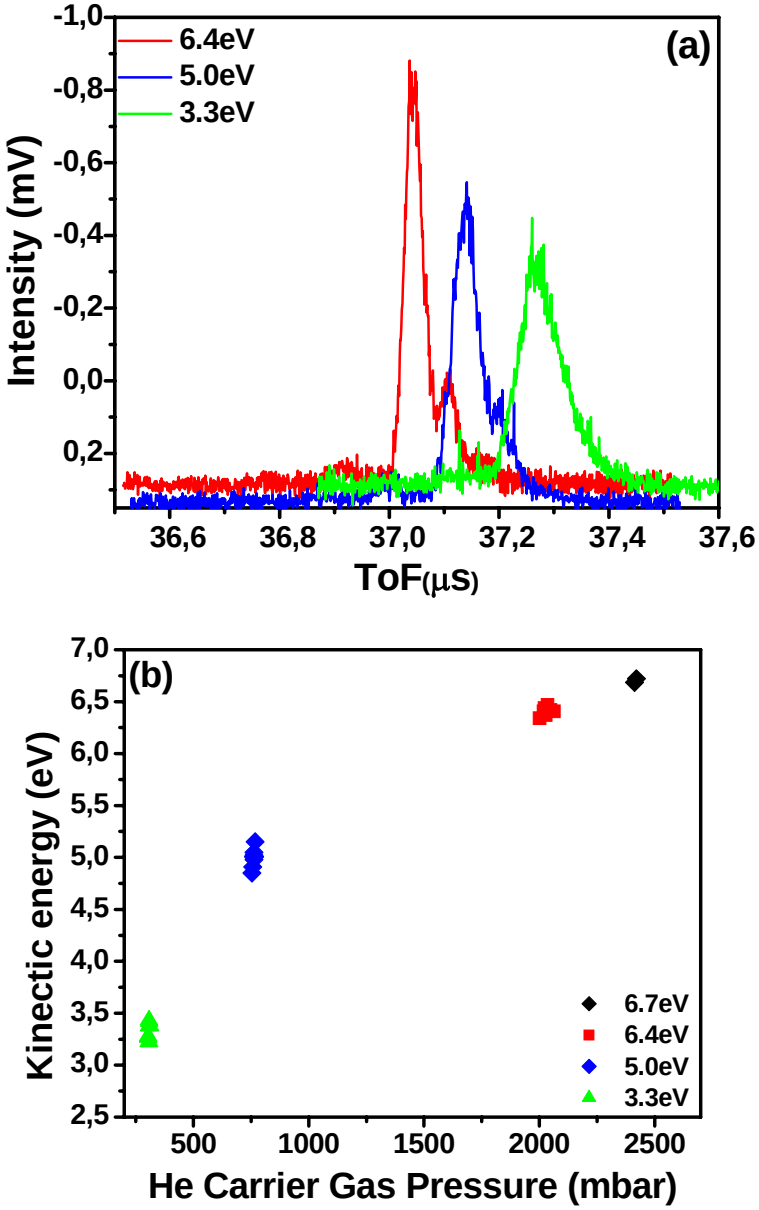

Figure 3-1: (a) Time of flight mass spectra of supersonic molecular beams of pentacene molecules: the peaks are centered at 37.04 μs, 37.14 μs and 37.26 μs correspond to average kinetic energies of 6.4 eV, 5.0 eV and 3.3 eV; (b) The molecular kinetic energy as a function of carrier gas pressure.

contrary, the molecular beam with kinetic energy of 3.3 eV has a large FWHM value of 0.08 μs corresponding to a velocity distribution, which is similar to that of a thermally sublimated pentacene molecular beam [25]. When keeping the nozzle at a constant temperature, the velocity of the pentacene in the molecular beam and hence its kinetic energy could be tuned by varying the carrier gas pressure, which in turn changes the concentration of seeded molecules in the carrier gas. To obtain the same flux in all experiments, the incident molecular beams have been adjusted in such a way as to achieve the same peak area in the mass spectra of all molecular beams. Figure 3-1 (b) shows the increase of the molecular kinetic energy as a function of helium pressure and indicates a very good reproducibility of the experimental conditions to obtain a certain kinetic energy with a certain carrier gas pressure.

3.2.3 Growth of pentacene submonolayers on SiO_x

The SiO_x substrates were first introduced in the entry lock, which was pumped to ultrahigh vacuum (7- 8×10^{-8} mbar) and then transferred one by one into the preparation chamber when they were needed for the growth experiments.

Purified pentacene powder of a dark blue colour (99.98%, purchased from Sigma Aldrich, Corp.) was further purified by vacuum sublimation under a temperature gradient [26]. This purification was carried out at 430 K for 70 hours in the dark to protect the molecules against UV degradation. The purified pentacene powder was carefully loaded into the quartz tube in the first vacuum chamber of the supersonic molecular beam system and outgassed for at least 3- 4 hours at a pressure of 3- 4×10^{-7} mbar before starting the experiments.

The supersonic molecular beam with a specified kinetic energy was generated by extraction through the nozzle under a pressure gradient formed between the inside and the outside of the source. Pentacene sublimation was achieved by sending a DC current (~ 8-9 A) through the tantalum foil wrapped around the quartz tube and heating it to ~ 480 K. To control the energy transfer in the collision between the molecules and helium atoms, the nozzle was heated to ~ 430 K by sending DC current (~ 1.1 A) through a tantalum filament placed closeby. Generally, it took about 2-3 hours to stabilize the experimental conditions. The SiO_x surface was

positioned vertically facing the incident supersonic molecular beam, which covered a spot with an area of 10 mm in diameter. All pentacene growth experiments described in this chapter were performed with the substrate at room temperature. With deposition times of 10, 20, 30 and 50 min we could monitor the evolution of pentacene submonolayer coverage for each kinetic energy of the molecular beam. The typical flux was about 6×10^{11} molecules/(s·cm^2) estimated from equation 3-1 [27] where P_0 is vapour pressure of thermally sublimated pentacene, T_0 the real temperature of pentacene during sublimation and *m* the mass of molecule.

$$I(0)\alpha\frac{P_0}{\sqrt{mT_0}} \qquad (3\text{-}1)$$

T_0 and P_0 [28] were measured in the experiment of pentacene thermal sublimation, where the sublimation rate was regulated to give the same peak area in the ToF spectra as those shown in figure 3-1(a). A growth rate of 1 ML/45 min as determined by a crystal microbalance and calibrated with the thickness measurement by *ex-situ* tapping mode AFM, was applied for all experiments and could be adjusted by simply changing the sublimation temperature. Four different kinetic energies (3.3 eV, 5.0 eV, 6.4 eV, and 6.7 eV) were obtained by properly tuning the helium carrier gas pressure while monitoring the flux of seeded pentacene molecules through ToF spectroscopy. The pressures for our beams were 300 mbar, 760 mbar, 2000 mbar and 2400 mbar. 6.7eV was the highest kinetic energy achievable in the experimental conditions used for the investigation presented in this chapter. After pentacene deposition the sample was transferred back to the entry lock and stored there in UHV and in the dark before further characterization.

One set of pentacene submonolayers was prepared by organic molecular beam deposition (OMBD) as described in reference [29]. The deposition rate was ~ 1 ML/45 min, as measured by a quartz crystal microbalance. The substrate was kept at room temperature during deposition.

The deposited pentacene submonolayers were imaged by *ex-situ* tapping mode atomic force microscopy, TM-AFM, (Multimode Scanning Probe Microscope, Digital Instruments, Veeco Metrology Group, U.S.A.) with a silicon tip with nominal radius less than 10 nm as scanning probe.

We selected five scanning regions around the centre of the deposition area and fixed the scanning size to 10×10 μm^2. The detailed analysis of AFM data was carried out with the WSxM software (version 8.7, Nanotec electronica S.L., Spain, see ref. 30). The statistical analysis of the AFM data was performed with the help of specific software (Origin 7.0, OriginLabs Inc., U.S.A.)

We also employed AFM to perform transverse shear microscopy (TSM) [31, 32, 33]. In this technique, a triangular shaped silicon nitride AFM tip (NP-20 Veeco Metrology and Instrument, U.S.A.) with a spring constant of 0.58 N m^{-1} is scanned in contact mode parallel to the cantilever's long axis. Like this one can measure the net transverse shear force, resulting from the changes in the tip-surface interaction when the tip is scanned over regions where the molecules pack with different orientation [33]. By mapping the variation in transverse shear force with colour contrast, we could qualitatively determine the crystallinity of a single molecular island or of the monolayer. 10×10 μm^2 TSM images were collected in parallel with the AFM height images for samples grown by OMBD and SuMBD presenting a nearly completed first monolayer.

3.3 Investigation of pentacene submonolayer growth

3.3.1 Formation of pentacene islands

Figure 3-2 presents TM-AFM micrographs illustrating the morphology of pentacene layers corresponding to ~ 0.3ML coverage and resulting from different growth conditions. All SuMBD samples (Fig. 3-2 (b-d)) consist typically of lobular islands with smooth edges, while the OMBD sample (Fig. 3-2 (a)) is characterized by islands with rougher edges as well as by the presence of smaller dendritic islands, as minority species. If one ignores the minority species, the samples grown by OMBD (Fig. 3-2 (a)) and by SuMBD with E_k = 3.3 eV (Fig. 3-2 (b)) are rather similar in that they both show a larger average island size and lower nucleation density than the samples grown by SuMBD at E_k = 5.0 eV and E_k = 6.4 eV, shown in Figs. 3-2 (c) and 3-2 (d), respectively.

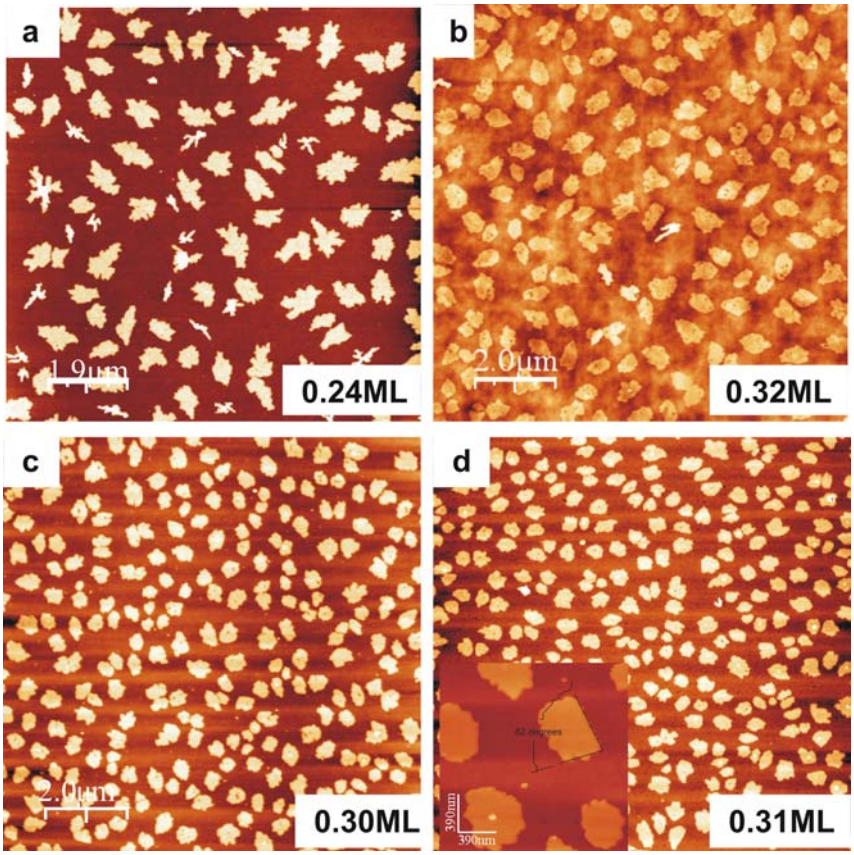

Figure 3-2: Tapping mode AFM (10×10 μm^2) micrographs of pentacene submonolayers grown by OMBD (a) and by SuMBD at E_k = 3.3 eV (b), E_k = 5.0 eV (c) and E_k = 6.4 eV (d). The inset of figure (d) shows the angle of 82° formed by two island edges.

The nucleation density (N) as a function of the kinetic energy of the impinging molecules, plotted in figure 3-3 (a), quantifies this observation. To derive N, the molecular island number was averaged from five AFM images collected in different regions on each sample, by using the flooding function in the WSxm 8.7 software. For the sample grown with pentacene at E_k = 6.4 eV, N is ~ 57% higher than for the OMBD sample and ~ 45% higher than for the SuMBD sample grown at E_k = 3.3 eV but it is only ~ 5% higher than for the SuMBD sample grown at E_k = 5.0 eV. We suggest that this difference is generated by the different

molecular surface diffusivity due to the different growth regimes. In fact, the experimental evidence indicates that pentacene monomers with high $E_{k,}$ ($\geq$ 5.0 eV) may sample many adsorption sites before being adsorbed or desorbed with roughly an equal probability to either integrate into a preformed islands or form a new nucleus on the empty surface in between the islands. On the other hand for samples grown with pentacene at low E_k, such as in OMBD and SuMBD with E_k = 3.3 eV, the probability for an incoming monomer to irreversibly integrate into the preformed molecular islands becomes dominant with respect to forming new nuclei in an uncovered substrate region [14].

We calculated the average island size for each sample from the sum of four island area histograms obtained from four AFM images collected in different regions of each sample. The sum histograms are presented in figure 3-3 (b) and the average island size is derived by fitting the data with a lognormal function. We found average island sizes of 0.13± 0.02 μm^2, 0.12 ± 0.01 μm^2 and 0.11 ± 0.01 μm^2 for SuMBD samples, where pentacene impinges with E_k = 3.3 eV, 5.0 eV and 6.4 eV. An average island size of 0.22 ± 0.07 μm^2 was determined for the OMBD sample.
From figure 3-3 (b), one clearly sees that the island size distribution becomes narrower and peaked at smaller values when the kinetic energy increases. This trend towards a more uniform island size that is characteristic of a changeover towards correlated island growth as proposed by S. Pratontep *et al* [34, 35], where the overlap area of the capture zones of neighbouring islands is large. The broader island size distribution is observed for the sample deposited with the 3.3 eV beam and with the thermal energy growth. An insight into the growth of pentacene islands from hyperthermal beams can be achieved by considering that it is a diffusion limited process [21,22]. When colliding with the surface, the initial kinetic energy of pentacene is converted (partially) into kinetic energy parallel to the surface via a complex mechanism involving inelastic molecule-molecule and molecule-surface energy transfer processes [36, 37, 38, 39]. It is therefore reasonable to assume, by extending consolidated growth models [21, 22, 23], that molecules with higher kinetic energy diffuse over longer distances before aggregating with other diffusing molecules or before being captured by pre-formed molecular islands. This would result in a more uniformly dispersed pattern of small molecular islands. On the contrary, molecules with a lower kinetic energy travel shorter distances on the surface and have a lower probability to form new

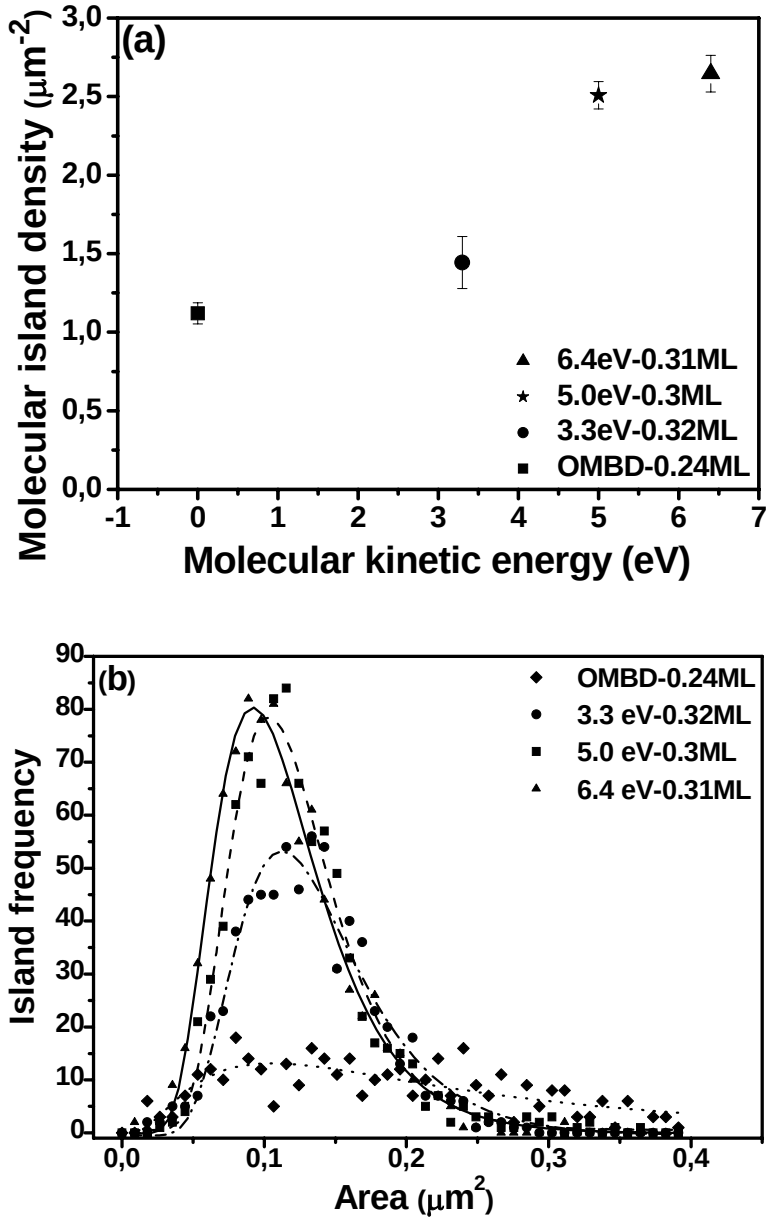

Figure 3-3: (a) Molecular island density obtained from submonolayers grown by OMBD and by SuMBD at E_k of 3.3 eV, 5.0 eV and 6.4 eV; (b) Molecular island size distribution for the same samples.

islands by colliding with other freely diffusing molecules at empty sites.

Another important issue that we investigated is the role played by the kinetic energy of the impinging pentacene molecules in determining the island shape. To this end we considered the islands at low coverage where coalescence has not started yet (see Fig. 3-2 (a-d)) and determined the fractal dimension for each growth condition. The island fractal dimension (D_f), as illustrated in figure 3-4 (a-d), is calculated by the area-perimeter relationship $P = kA^{\frac{D_f}{2}}$, proposed in [40], where P the island perimeter, A its area, k a scaling constant and D_f the fractal dimension. When the $D_f = 2$ it means the measured structure has the typical fractal shape because of the highest self similarity, which means that the object is exactly or approximately similar to a part of itself, such like the coastline. The mean D_f turns out to be decreasing from 1.40 ± 0.05 for the SuMBD samples grown at $E_k = 3.3$ eV to 1.39 ± 0.04 for those deposited with $E_k = 5.0$ eV and 1.30 ± 0.03 for the layer formed when $E_k = 6.4$ eV. The data points are more and more scattered as E_k decreases (see Fig. 3-4(c)) due to the larger dispersion in island size distribution but the D_f values never approach those typical of a fractal island structure, in agreement with the island morphology observable in Fig. 3-2. For the islands grown by OMBD, the mean D_f can not be correctly derived by one linear fit because of the presence of two types of islands (see discussion Fig. 3-2 (a) above) causes a much larger scattering of the data points. However, as shown in figure 3-4 (d), if two different linear fittings are carried out for the majority and the minority species of islands, one obtains a large mean $D_f = 1.69 \pm 0.05$ for the small dentritic islands (reversed filled triangles in the figure), and D_f of 1.60 ± 0.05 for the data corresponding to the larger islands (labeled by filled diamonds). Dendritic or fractal islands occur naturally during growth in systems where island edge diffusion is restricted.

To better understand how the molecular island shape is correlated with the kinetic energy of the impinging molecules, we performed a statistical analysis of the ratio (R) between the large (L_L) and small (L_s) dimensions of pentacene islands, the result of which is plotted in figure 3-5. The average R values were obtained by measuring 50 molecular islands randomly chosen for each sample. Although the error bars are relatively large, there is an indication of a trend towards the formation of anisotropic

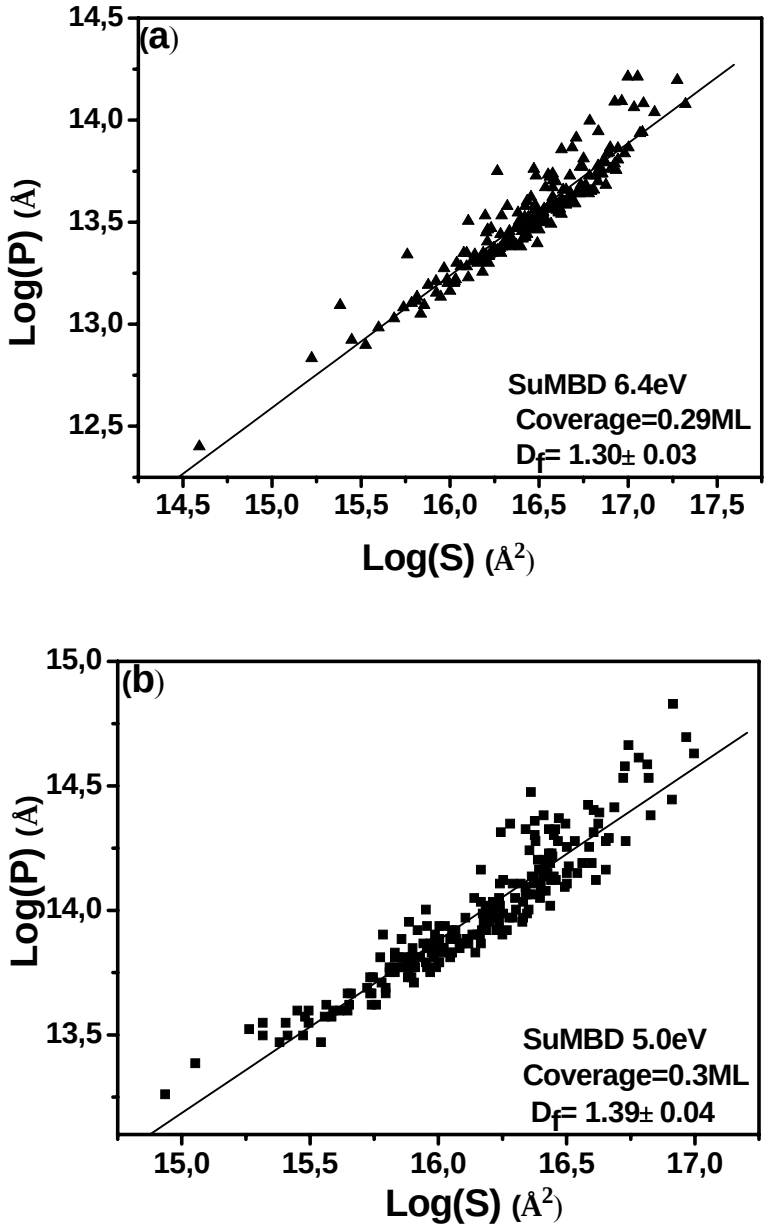

Figure 3-4: Mean fractal dimension (D_f) obtained from (a) sample prepared by SuMBD at 6.4 eV with $D_f = 1.30 \pm 0.03$; (b) sample prepared by SuMBD at 5.0 eV with $D_f = 1.39 \pm 0.04$; S is the measured area and P is the perimeter of the individual island.

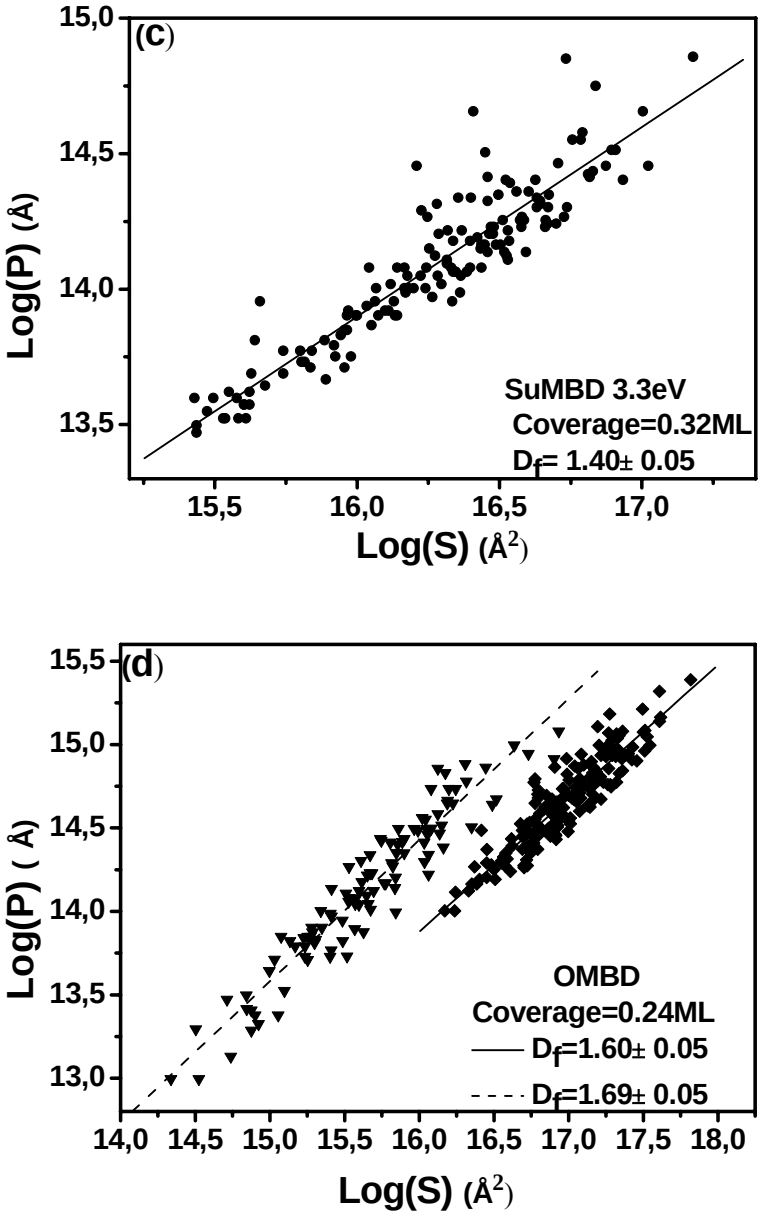

Figure 3-4: Mean fractal dimension (D_f) obtained from (c) sample prepared by SuMBD at 3.3 eV with $D_f = 1.40 \pm 0.05$; (d) sample prepared by thermal evaporation with the $D_f = 1.60 \pm 0.05$ and $D_f = 1.69 \pm 0.05$. S is the measured area and P is the perimeter of the individual island.

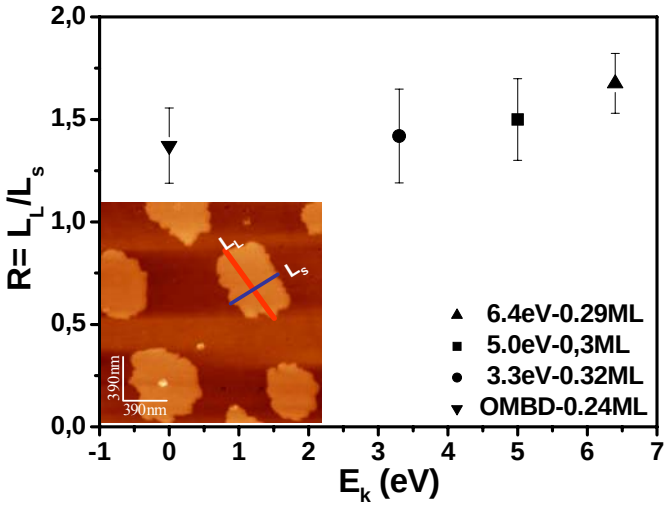

Figure 3-5: Statistic measurement of the ratio (R) between the large length (L_L) and small length (L_s) of deposited pentacene islands in different submonolayers prepared by OMBD and by SuMBD at E_k of 6.4 eV, 5.0 eV and 3.3 eV. Inset shows the definition of L_L and L_s.

islands when E_k increases. This anisotropic island formation cannot be due to an anisotropy in surface diffusion of pentacene since SiO_x is chemically inert and amorphous, we suggest instead that it is caused by the molecular diffusion at island edges, which can also trigger the formation of a non-fractal structure [41, 42].

A quantitative assessment of the initial growth process was achieved by determining the critical nucleus, *i* (*i*+1 = number of molecules forming a stable nucleus), on the basis of the general scaling function (3-2) introduced by Amar and Family [23] and extended to pentacene growth by Ruiz *et al.* [21], and hence reproposed by Tejima *et al.* and Stadlober *et al.* [43, 44]. C_i and b_i are constants determined by hypergeometrical equations (3-3), (3-4) for i= 0 to 3 that assure normalization and proper asymptotic behaviour of $f_i(u)$; $u = a/A(\theta)$ (a is the area of each molecular island extracted in the pentacene submonolayer, $A(\theta)$ is the average island size); Γ is the gamma function, which is an extension of the factorial function to real and complex number.

$$f_i(u) = C_i u^i e^{-ib_i u^{\frac{1}{b_i}}} \quad (3\text{-}2);$$

$$(ib_i) = \frac{\Gamma[(i+2)b_i]}{\Gamma[(i+1)b_i]} \quad (3\text{-}3);$$

$$(C_i) = \frac{[(ib_i)^{(i+1)b_i}]}{[b_i \Gamma[(i+1)b_i]} \quad (3\text{-}4);$$

Figure 3-6(a) compares the properly normalized island size distributions of pentacene submonolayers grown at E_k= 3.3 eV and E_k= 6.4 eV with the predictions of the general scaling model calculated for i = 1, 2 and 3. For the highest E_k used here, we systematically observed a much better agreement for i=2, as confirmed by the χ^2 criterion. At E_k lower than about 5.5- 6.0 eV, the experimental island size distribution is better reproduced by the i=3 distribution, as was previously reported for submonolayers deposited on similar substrates and temperatures by thermal sublimation [21, 43, 44]. Analyzing series of different sets of data by best fitting procedures, we confirmed that the critical nucleus decreases from 3 to 2 over a threshold of E_k of the molecules in the beam as shown in figure 3-6(b).

The diffusion growth model confirms the important role played by E_k in regulating the formation and the growth of pentacene islands. The probability that three free molecules with high surface diffusivity meet is higher than that four free molecules with lower diffusivity come together and this is the basic mechanism that explains the high nucleation density with a dispersive nuclei distribution obtained for samples grown at $E_k \geq 5.0$ eV in the low coverage regime. Furthermore, the high nucleation density can proportionally reduce the average island-island distance, which is favourable to the growth of the highly correlated molecular islands. Since the growth is diffusion mediated, such a higher density shifts the onset of the island-island coalescence process to a much earlier stage. The final outcome is a process where the smaller and more mobile islands can merge easier in a crystalline film with reduced number of grain boundaries.

When comparing our findings to the ones of Killimpally *et al.* [20],

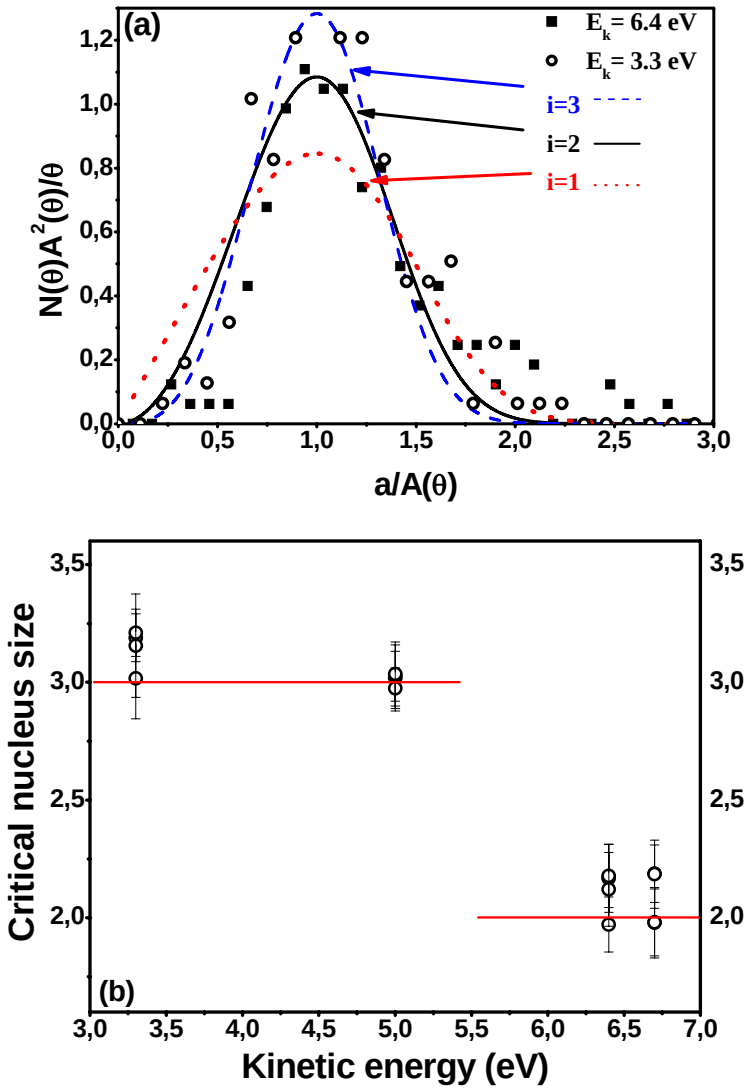

Figure 3-6: (a) The properly normalized island size distributions of films formed at E_k=6.4 eV (■) and E_k=3.3 eV (○) indicate different critical nucleus sizes, respectively i=2 and i=3, in the framework of the scaling function predictions reported in the plot as broken line (i=3), continuous line (i=2) and dotted line (i=1) (see text), N(θ) is island size distribution, A(θ) is average island size and θ is coverage; (b) Critical nucleus sizes extracted from the experimental island distributions as a function of E_k of pentacene molecules, for 10 min deposition time. The lines for i=2 and i=3 are shown as guide the eye. A transition between two different growth regimes is observed at ~5.5-6.0 eV.

one notices important differences in the E_k-dependence of the coverage and of the morphologies as well as of the critical nucleus. Our results demonstrate that remarkably different regimes of growth can be achieved in SuMBD by carefully tuning kinetic energy and flux (the growth rates in our experiments were about a factor 50 lower than that in [20]).

3.3.2 Morphological evolution of the pentacene submonolayer

Figure 3-7 shows the TM-AFM micrographs of layers obtained with the same deposition conditions as in Fig. 3-2 but for longer deposition times. When the coverage increases up to ~ 0.5 - 0.65 ML, island coalescence is observed for all samples (Fig. 3-7 (a-d)). From the surface morphology one concludes that second layer nucleation occurs at this coverage for the OMBD grown pentacene layer in agreement with a previous report [14]. On the other hand, second layer nuclei are extremely rare for all SuMBD samples. When further extending the deposition to a time where the coverage of all samples is close to completion of their first monolayer (see figure 3-7 (e-h)), all pentacene islands are connected to each other via coalescence, while grain boundaries appear. For all samples the monolayer is 1.5±0.2 nm thick confirming that pentacene molecules

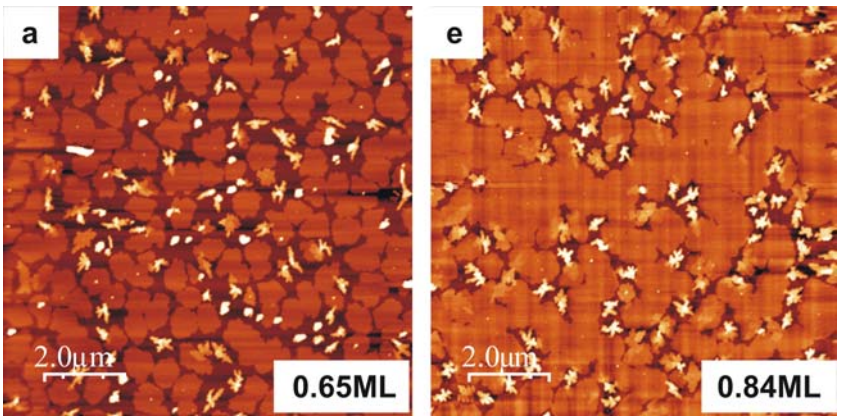

Figure 3-7: Tapping mode AFM (10×10 μm^2) micrographs of pentacene submonolayers grown by OMBD (a and e)

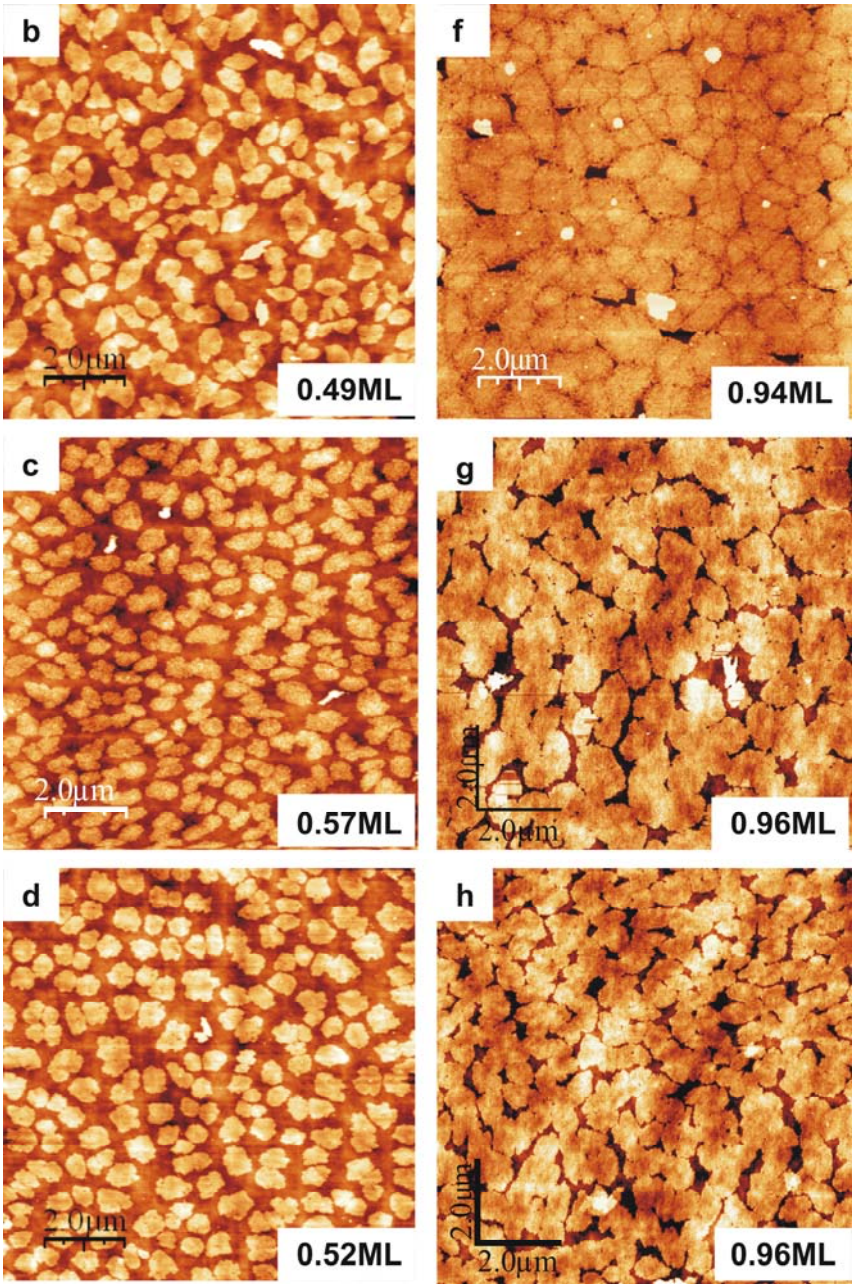

Figure 3-7: Tapping mode AFM (10×10 μm^2) micrographs of pentacene submonolayers grown by SuMBD at E_k = 3.3 eV (b and f), E_k = 5.0 eV (c and g) and E_k = 6.4 eV (d and h).

pack upright. Second and third layer nuclei typical of the Vollmer-Weber growth mode are now very clearly visible for the OMBD sample. While a few second layer islands are also present on top of the first layer of SuMBD sample grown at E_k = 3.3 eV (Fig. 3-7 (f)), SuMBD samples produced at higher kinetic energies still hardly show any second layer formed on the top of first monolayer implying the Stransky- Krastanov growth mode. This is a strong indication that at high E_k the diffusivity of pentacene, after landing on top of the first layer islands, is sufficiently high to always sample the island edge and its energy is large enough to overcome the edge barrier or "Schwoebel barrier" [45], which otherwise hinders the impinging pentacene from moving down to the substrate. This assumption receives support from the fact that we often observe an island shape as shown in the inset of figure 3-2 (d): the angle of ~ 82°, formed by two island edges is very close to that formed by the *a*-*b* lattice vectors in the pentacene (001) crystal plane as reported by J. E. Northrup *et al.* in the calculation of pentacene packing in the single layer [46].

3.3.3 Crystallinity of first pentacene monolayer

To learn more about the quality of the first monolayer and in particular to determine the size of single crystal domains, we carried out transverse shear microscopy studies. When scanning over the surface of a polycrystalline layer, the tip feels a different friction on crystal domains with different pentacene orientation and packing. The distribution of crystal domains is identified by the friction force contrast that is visualized by different colours.

Figure 3-8 compares the contact mode AFM micrographs where colour represents height on sample surface together with the corresponding TSM images for samples grown by OMBD and by SuMBD at E_k of 3.3 eV and 6.4 eV. The OMBD sample (Fig. 3-8 (a, b)) shows a typical polycrystalline structure with random in-plane orientation of the single crystalline domains in the first monolayer. The domain size reaches 1-2 μm that corresponds very closely to the average size of isolated pentacene islands before the onset of aggregation. The coalescence process seems not to influence the orientation alignment of the merging islands (see arrows in figure 3-8 (b)), in agreement with previous findings [33] so that a large number of grain boundaries is present in the first monolayer. The second

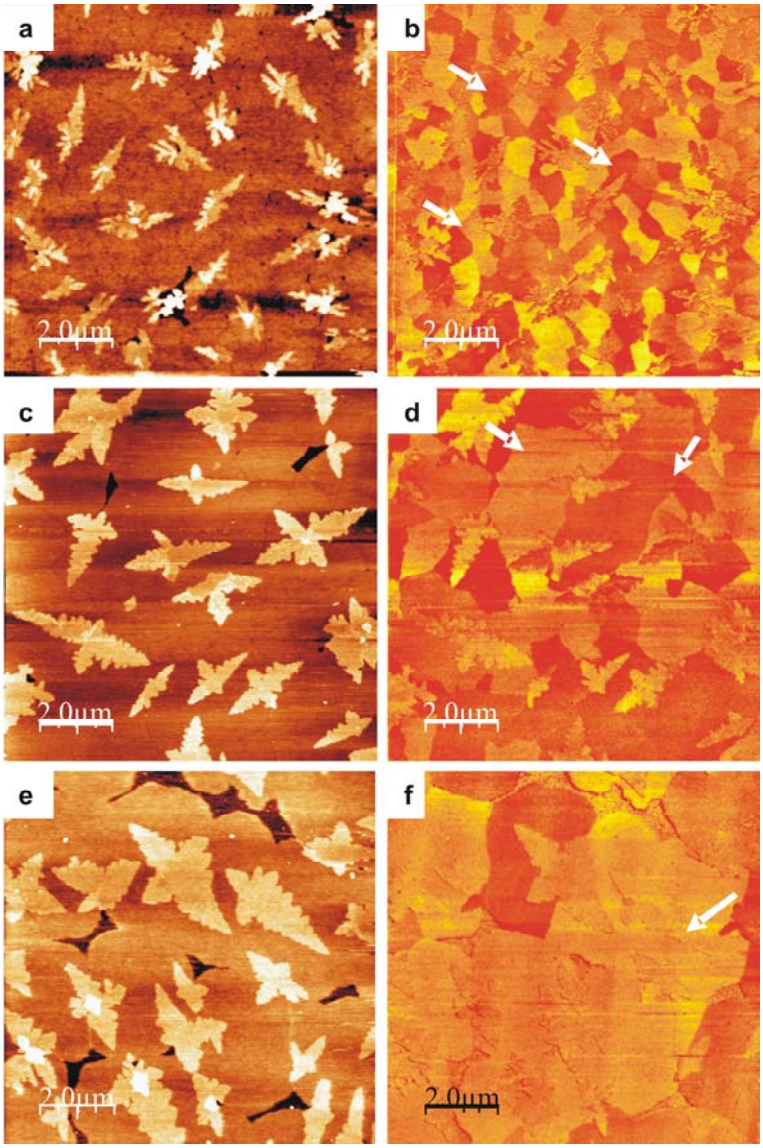

Figure 3-8: Contact mode AFM height images and transverse shear force micrographs of pentacene monolayers grown on a SiO_x surface by OMBD ((a) and (b), respectively) and by SuMBD where the molecules impinge on the surface with a kinetic energy of 3.3 eV ((c) and (d), respectively) and of 6.4 eV ((e)and (f), respectively). White arrows point to single crystal grains.

layer islands, which cover about 1/5 of the monolayer, show a typical dendritic shape and most of them are composed of several crystalline domains. The SuMBD sample grown at E_k = 3.3 eV (Fig. 3-8 (c, d)) displays larger single crystalline domains (see arrows in figure 3-8 (d)) with more regular shape and sharp edges. The islands have merged after coalescence and hence the number of grain boundaries are much less than in the OMBD grown sample. Furthermore, in the second layer, covering about 1/4 of the first one, the percentage forming single-crystalline islands is much higher than in the OMBD sample. In the film grown at E_k = 6.4 eV (Fig. 3-8 (e, f)) the size of single crystal domains in the first monolayer increases dramatically. The largest single crystalline domain within the 10×10 μm^2 scanning area, indicated by the arrow in Fig 3-8 (f), spans 9-10 μm. The second layer covers about 1/3 of the monolayer and all of its molecular islands are larger than those of the other two samples and show a single crystal structure. There is hence a strong indication that the majority of the second layer islands grow epitaxially on the underlying crystal domain since they show the same friction force contrast as the layer below. This implies that at high kinetic energies of the impinging pentacene, the island growth is highly correlated with a mechanism that favours orientational alignment of the islands before coalescence occurs. On the basis of our experimental evidence and in particular in order to explain the generation of the observed large domains, we speculate that the reorientation of entire islands should be part of the energy dissipation mechanisms characteristic of SuMBD growth. Theoretical studies would be helpful to further clarify this question.

3.4 Conclusions

We have demonstrated that the kinetic energy of pentacene molecules, landing on a silicon oxide surface, plays a crucial role in determining island structure, shape, size distribution and even the quality of the first monolayer as well as of upper layers. By increasing E_k the island structure reverts from fractal to non-fractal structure in the low coverage regime, the island shape becomes more anisotropic due to the molecular diffusion along the island edges and the island size becomes more uniform because of correlate island growth. We interpreted the impact of E_k in terms of the diffusion mediated model, and found that the critical nucleus reduces

from i=3 (typical for OMBD) to i=2 for E_k>5-6 eV. The completion of the first layer before the second one starts to form has been clearly observed from all samples grown by SuMBD indicating the Stransky- Krastanov growth mode. The quality of first monolayer is greatly improved when $E_k \geq$ 5.0 eV presenting very few grain boundaries. The formation of single crystalline domains spanning over up to ~10 μm in the monolayer is successfully achieved in the growth at the high kinetic energies. To explain the formation of single crystalline domains spanning over up to ~ 10 μm in the monolayer, we suggest that this is consistent with the reorientation of entire island, which is part of the energy dissipation at these high kinetic energies, during coalescence.

References

1. C. D. Dimitrakopoulos, and P. R. L. Malenfant, Adv. Mat. **14,** 99 (2002).
2. S. Lee, B. Koo, J. Shin, E. Lee, H. Park, H. Kim, Appl. Phys. Lett. **88**, 162109 (2006).
3. A. Di Carlo, F. Piacenza, A. Bolognesi, B. Stadlober and H. Maresch, Appl. Phys. Lett. **86**, 263501 (2005).
4. R.A.Street, D. Knipp and A.R. Volkel, Appl. Phys. Lett. **80**, 1658 (2002).
5. B. Nickel, R. Barabash, R. Ruiz, N. Koch, A. Kahn, L. C. Feldman, R.F. Haglund and G. Scoles, Phys. Rev. B, **70** 125401 (2004).
6. A. C. Mayer, R. Ruiz, R. L. Headrick, A. Kazimirovc and G. G. Malliaras, Organ. Electr. **5**, 257 (2004).
7. A. C. Mayer, A. Kazimirov and G. G. Malliaras, Phys. Rev. Lett. **97**, 105503 (2006).
8. S. Schiefer, M. Huth, A. Dobrinevski and B. Nickel, J. Am. Chem. Soc. **129**, 10316 (2007).
9. G. Horowitz, J. Mater. Res. **19,** 1946 (2004).
10. S. Pratontep, F. Nuesch, L. Zuppiroli and M. Brinkmann, Phys. Rev. B **72**, 085211 (2005).
11. M. Kitamura and Y. Arakawa, J. Phys Condens. Matter **20**,124011 (2008).

12. F.-J. Meyer zu Heringdorf, M.C. Reuter and R.M.Tromp, Nature **412**, 517, (2002).
13. B. Stadlober, U. Haas, H. Maresch and A. Haase, Phys. Rev. B **74**, 165302, (2006).
14. R. Ruiz, B. Nickel, N. Koch, L.C. Feldman, R.F. Haglund, A. Kahn and G. Scoles, Phys. Rev. B **67**, 125406, (2003).
15. S. Iannotta, T. Toccoli, J. Polymer Sci. B, **41**, 2501 (2003).
16. L. Casalis, M. F. Danisman, B. Nickel, G. Bracco, T. Toccoli, S. Iannotta and G. Scoles, Phys. Rev. Lett. **90**, 206101 (2003).
17. F. De Angelis, T. Toccoli, A. Pallaoro, N. Coppedè, L. Mariucci, G. Fortunato and S. Iannotta, Synth. Met. **146**, 291 (2004).
18. F. Dinelli, M. Murgia, P. Levy, M. Cavallini, F. Biscarini and D.M. De Leeuw, Phys. Rev. Lett. **92,** 116802 (2004).
19. R. Ruiz, A. Papadimitratos, A. C. Mayer, G. G. Malliaras, Adv. Mat. **17**, 1795, (2005).
20. A. S. Killampalli, T. W. Schroeder and J. R. Engstrom, Appl. Phys. Lett. **87,** 033110 (2005).
21. R. Ruiz, B. Nickel, N. Koch, L. C. Feldman, R. F. Haglund Jr., A. Kahn, F. Family and G. Scoles, Phys. Rev. Lett. **91**, 136102 (2003).
22. R. Ruiz, D. Choudhary, B. Nickel, T. Toccoli, K.-C. Chang, A. C. Mayer, P. Clancy, J. M. Blakely, R. L. Headrick, S. Iannotta, and G. G. Malliaras, Chem. Mater. **16**, 4497 (2004).
23. J. G. Amar and F. Family, Phys. Rev. Lett. **74**, 2066 (1995).
24. K. L. Mittal, Ed., " Contact angle wettability and adhesion" (VSP, Utrecht, 1993).
25. G. Scoles, Atomic and Molecular Beam Methods, Oxford University Press (1988).
26. O. D. Jurchescu, J. Baas and T.M. Palstra, Appl. Phys. Lett. **84**, 3061 (2004).
27. T. Toccoli, Organic Thin Film Growth by Supersonic Molecular Beams for Device Application, PhD thesis, University of Groningen (2007).
28. C. G. De Kruif, J. Chem. Thermodynamics, **12**, 243 (1980).
29. R. Ruiz, B. Nickel, N. Koch, L.C. Feldman, R.F. Haglund, A. Kahn and G. Scoles, Phys. Rev. B **67**, 125406, (2003).
30. I. Horcas, R. Fernandez, J.M. Gomez-Rodriguez, J. Colchero, J. Gomez-Herrero, and A.M. Baro, Rev. Sci. Instrum. **78,** 013705 (2007).

31. R. M. Overney, H. Takano, Fujihira, W. Paulus and H. Ringsdorf, Phys. Rev. Lett. **72**, 3546 (1994).
32. J. A. Last and M. D. Ward, Adv. Mater. **8**, 730 (1996).
33. K. Puntambekar, J. Dong, G. Haugstad and C. D. Frisbie, Adv. Fun. Mater. **16**, 879 (2006).
34. S. Pratontep, M. Brinkmann, F. Nuesch and L. Zuppiroli, Phys. Rev. B **69**, 165201, (2004).
35. M. Brinkman, S.Pratontep and C. Contal, Surface Science **600**, 4712 (2006)
36. C. T. Rettner, D. J. Auerbach, J. C. Tully and A. W. Kleyn, J. Phys. Chem. **100**, 13021, (1996).
37. C. T. Reeves, B. A. Ferguson, C. B. Mullins, G.O. Sitz, B. A. Helmer and D. B. Graves, J. Chem. Phys. **111**, 7567 (1999).
38. F. O. Goodman and H. Y. Wachman, Dynamics of Gas Surface Scattering (Academic Press, New York and London, 1976).
39. S. Iannotta, C. Gravili, A. Boschetti, A. Cagol, M. Cacciatore, Chem. Phys. **194**, 133 (1995)
40. P. A. Burrough, Principles of geographical systems for land resources assessment. Clarendon, Oxford (1986).
41. J. G. Amar, F. Family and M. N. Popescu, Comp. Phys. Comm. Vol. 146, 1 (2002).
42. G. Rosenfeld, R. Servaty, C. Teichert, B. Poelsema and G. Comsa, Phys. Rev. Lett. 71, 895 (1993).
43. M. Tejima, K. Kita, K. Kyuno and A. Toriumi, Appl. Phys. Lett. **85**, 3746 (2004).
44. B. Stadlober, U. Haas, H. Maresch and A. Haase, Phys. Rev. B **74**, 165302 (2006).
45. R. L. Schwoebel, J. Appl. Phys. **40**, 614 (1969).
46. J.E. Northrup, M. L. Tiago and S. G. Louie, Phys. Rev. B **66**,121404 (2002).